Science Advances

AAAS

advances.sciencemag.org/cgi/content/full/4/6/eaat1084/DC1

Supplementary Materials for

Superconductivity with twofold symmetry in $Bi_2Te_3/FeTe_{0.55}Se_{0.45}$ heterostructures

Mingyang Chen, Xiaoyu Chen, Huan Yang, Zengyi Du, Hai-Hu Wen

Published 8 June 2018, *Sci. Adv.* **4**, eaat1084 (2018)
DOI: 10.1126/sciadv.aat1084

This PDF file includes:

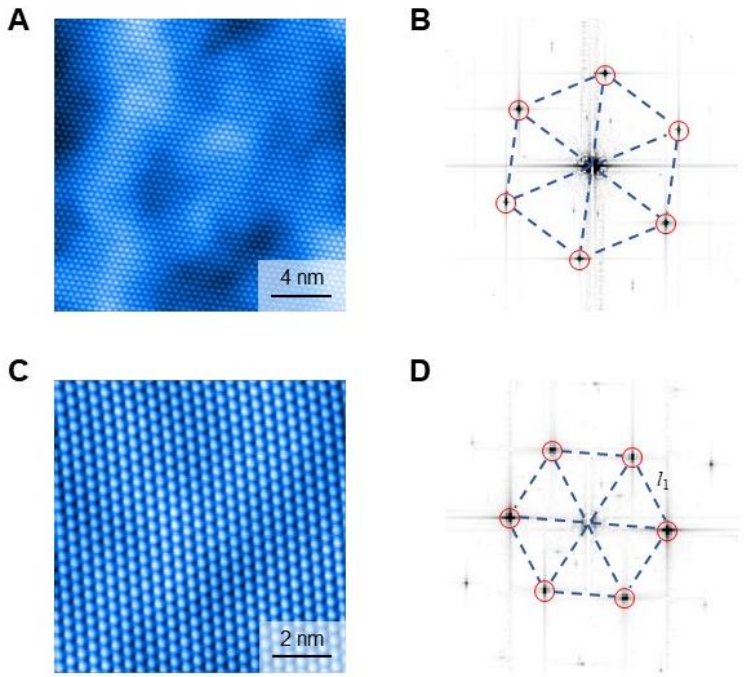

fig. S1. Atomically resolved topographies and Fourier transform images of Bi_2Te_3 thin films with thicknesses of 1 and 2 QLs. Topographies and the corresponding Fourier transform images of Bi_2Te_3 film with 1 QL (**A**, **B**) and 2 QL (**C**, **D**) thickness. One can see that the crystalline lattice of 1 QL and 2 QL are all hexagonal verified by the sharp and highly symmetric six Bragg spots enclosed by the red circles. The measuring conditions are (A) V_{bias} = 10 mV, I_t = 100 pA, (C) V_{bias} = 30 mV, I_t = 300 pA.

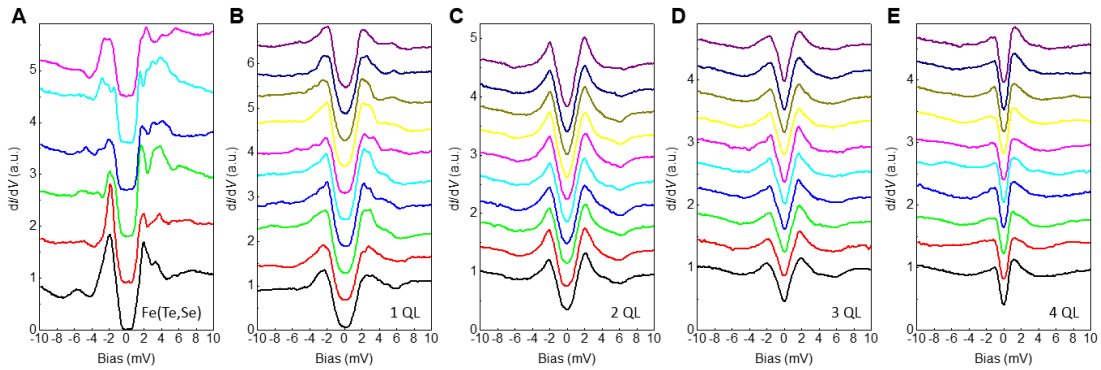

fig. S2. Series of tunneling spectra measured on $FeTe_{0.55}Se_{0.45}$ and Bi_2Te_3 thin films. All the spectra are measured at 0.4 K and zero magnetic field. The data were taken along lines with lengths of 10, 27, 68, 68, and 39 nm, respectively. Setpoint conditions V_{set} = 10 mV, I_{set} = 50 pA. One can see that the tunneling spectra become more homogeneous on the 2QL and thicker films of Bi_2Te_3.

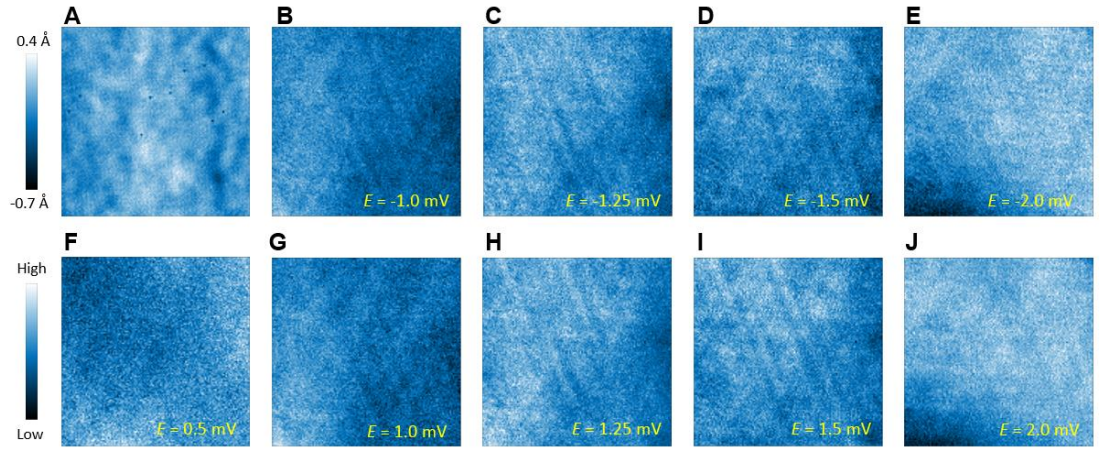

fig. S3. Real-space QPI patterns at series of energies on the 2-QL $Bi_2Te_3/FeTe_{0.55}Se_{0.45}$ heterostructure. (**A**) Topography of the view for QPI measurement. The size is 84 × 84 nm^2 with 128 × 128 pixels. (**B**-**J**) QPI image in real space measured at 0.4 K with V_{set} = 10 mV and I_{set} = 50 pA.

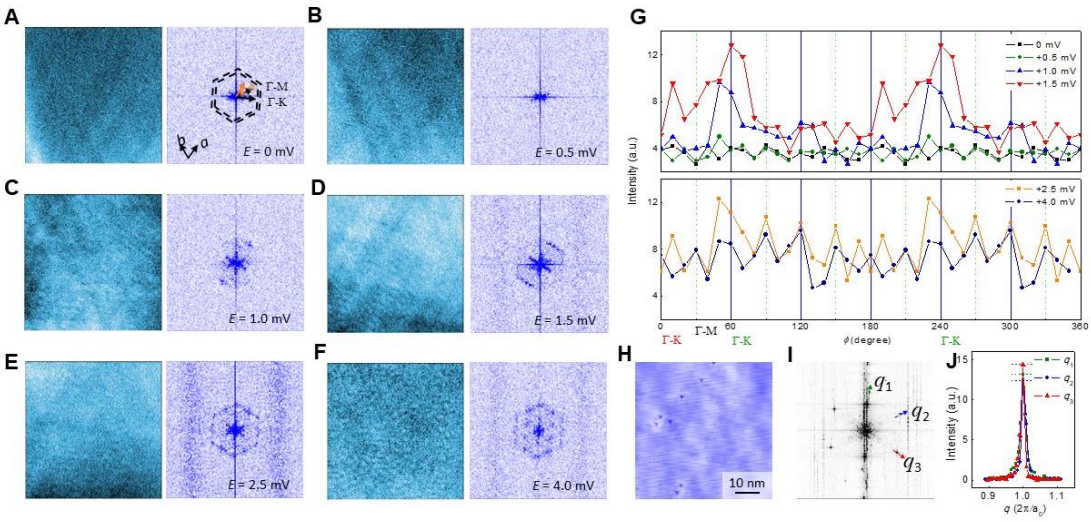

fig. S4. Control experimental QPI results on the 2-QL $Bi_2Te_3/FeTe_{0.55}Se_{0.45}$ heterostructure. (**A**-**F**) The QPI and corresponding FT-QPI images with the real-space area of 56 × 56 nm^2 (V_{set} = 10 mV, I_{set} = 50 pA). (**G**) The averaged FT-QPI intensity per pixel in the *q*-space within the band bounded by the two parallel dashed hexagons in A with increment of every 10 degrees. The initial angle of ϕ is defined from one Γ-K direction as marked by a red arrow in A. (**H**) Topography of the view for QPI measurement. (**I**) Fourier transformation of the topography. (**J**) *q* dependence of the absolute value along different arrows crossing Bragg peak patterns in Fourier transform image I. The peak amplitudes are very close to each other with the max intensity difference of about 16%.

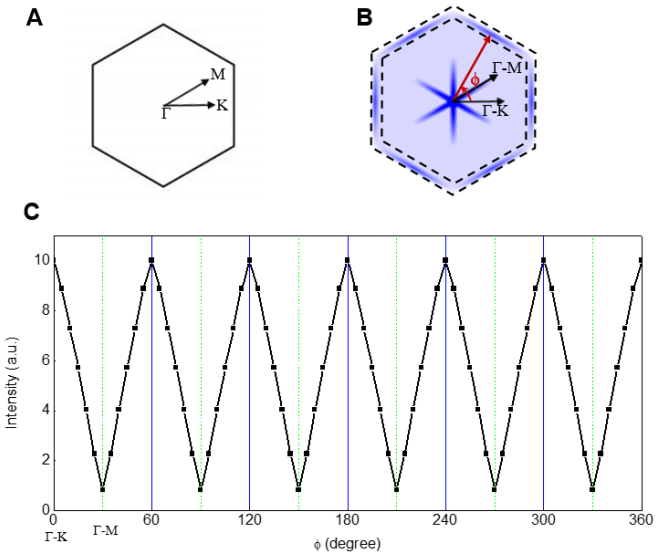

fig. S5. Simulation of FT-QPI pattern from a 2D hexagonal Fermi surface. (**A**) Schematic plot of 2D hexagonal Fermi surface. The DOS is assumed as a constant everywhere around the Fermi surface. (**B**) Theoretical simulation of QPI scattering intensity by applying self-correlation to A. (**C**) The averaged FT-QPI intensity per pixel in the *q*-space within the band bounded by the two parallel dashed hexagons in B with increment of every 5 degrees. The initial angle of ϕ is defined as one of the Γ-K directions.

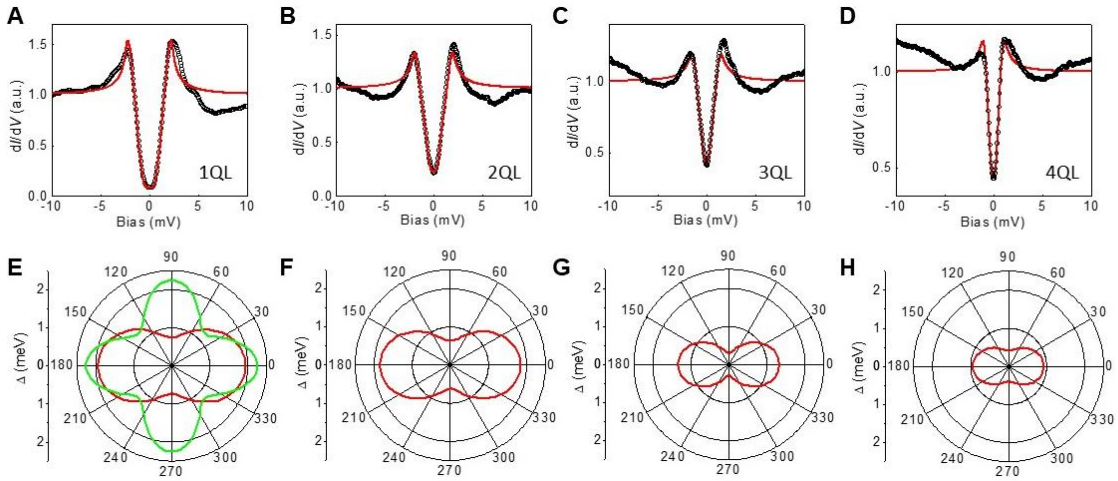

fig. S6. Typical tunneling spectra and theoretical fitting results. (**A-D**), Experiment data (solid symbols) and corresponding fitting curves (red lines) measured on 1 to 4 QL $Bi_2Te_3/FeTe_{0.55}Se_{0.45}$ heterostructures. (**E-H**), Gap functions used for fitting, respectively. For the 1QL $Bi_2Te_3/FeTe_{0.55}Se_{0.45}$ film, as shown in E, a combination of two gaps, one twofold (red) and one fourfold (green) symmetry, are needed to fit the data. For thicker films, one gap with twofold symmetry can give rise to a good fit.

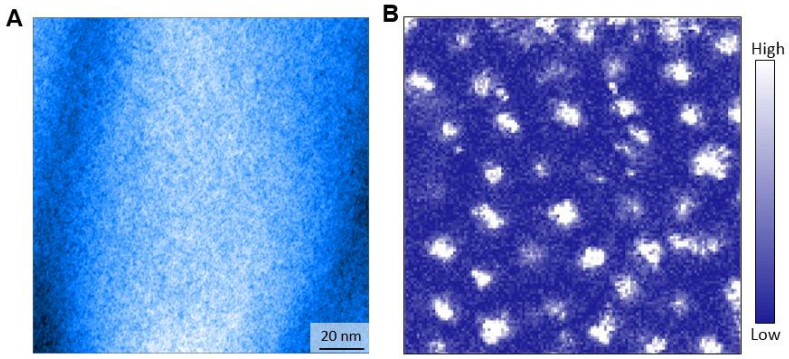

fig. S7. Vortex image on $FeTe_{0.55}Se_{0.45}$ substrate without Bi_2Te_3 film. (**A**) Topography of $FeTe_{0.55}Se_{0.45}$ substrate, the size of the image is 150 × 150 nm^2. (**B**) Vortex image measured by zero-bias conductance map at 0.4 K and 4.0 T (V_{set} = 10 mV, I_{set} = 50 pA). The shapes of the vortices are roughly round without any trace of elongation.

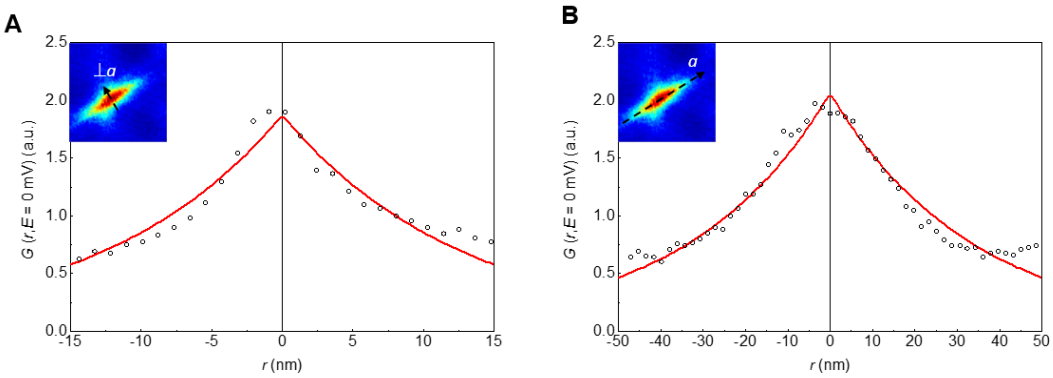

fig. S8. The spatial evolution of differential conductance across the elongated vortex. The experimental data (black circles) are fitted by an exponential decay formula (red lines), and we can obtain different coherence length of $\xi_{\perp a}$ = 12.7 nm, $\xi_{\parallel a}$ = 33.5 nm. The insets show the related vortex images.

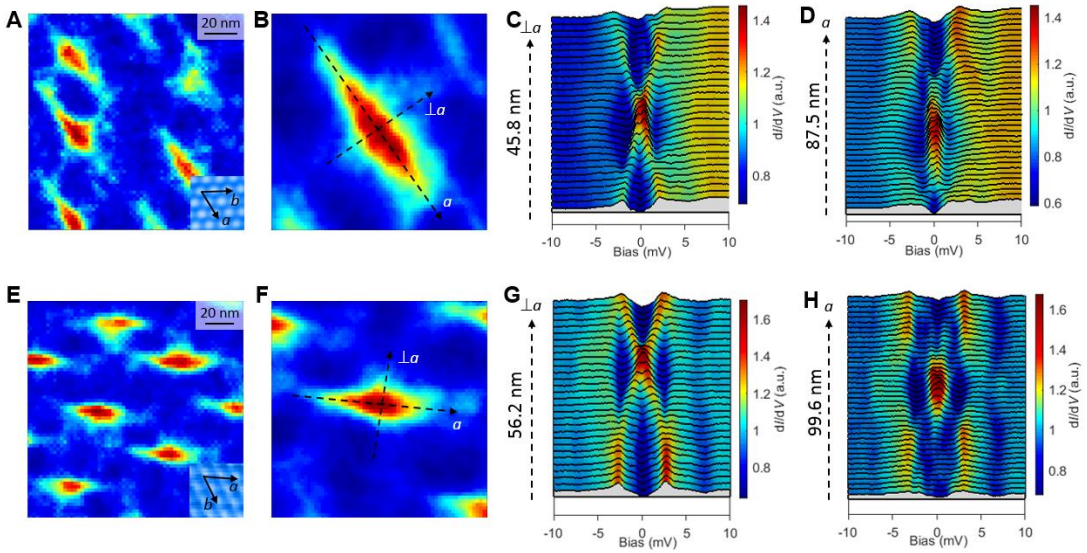

fig. S9. The control experiments of the elongated vortices. (**A**-**D**) Vortex images and bound states measured at different places on the same sample. (**E**-**H**) Vortex images and bound states measured on a different $Bi_2Te_3/FeTe_{0.55}Se_{0.45}$ heterostructure. All the vortices show elongated shape along one of the crystalline axis. The spatial evolution of the vortex bound states look similar. Setpoint parameters V_{set} = 10 mV, and I_{set} = 50 pA.

table S1. SC gap functions and fitting parameters used in the fitting to the tunneling spectra measured on Bi_2Te_3 with different thicknesses at 0.4 K.

Thickness	Γ (meV)	Δ (meV)	α
1QL	0.11	$\Delta_1 = 2.25(0.23\cos4\phi+0.77)$	52%
	0.11	$\Delta_2 = 1.94(0.31\cos2\phi+0.69)$	48%
2QL	0.25	$\Delta = 1.85(0.33\cos2\phi+0.67)$	100%
3QL	0.26	$\Delta = 1.35(0.39\cos2\phi+0.61)$	100%
4QL	0.31	$\Delta = 0.93(0.28\cos2\phi+0.72)$	100%